Chapter 5 Corrosion Behaviour of Additively Manufactured Ti-6Al-4V Alloy

In this chapter, corrosion studies are discussed in detail. Corrosion is performed to check the formation of oxides on the surface of additively manufactured Ti-6Al-4V alloy. Potentiodynamic polarization and electrochemical impedance spectroscopy tests were performed for corrosion test. This chapter describes the microstructural characterization and XPS analysis to evaluate the corroded surfaces.

5.1 Results and discussion

5.1.1 Electrochemical analysis of as-built and heat-treated AM samples

Figure 5.1 presents Tafel plots of the AB and HT samples in Ringer's solution. Tafel plot represents the relationship between electrode potential relative to SCE on *y*-axis and log current density on *x*-axis. Tafel plot is used for estimating corrosion rate. From the plots, it is noticed that the curve of heat-treated samples has shifted towards lower current density in comparison to the as-built samples, indicating that the electrochemical behaviour of the HT samples differs.

The corrosion potential (E_{corr}) is the potential at which the rate of anodic reactions and cathodic reactions is equal. The current density (i_{corr}) during corrosion may be obtained by extrapolating cathodic section of an individual plot to E_{corr}. Table 5.1 lists the i_{corr} and E_{corr} values obtained from the plots (Figure 5.1). According to the Tafel plots, the passive region is also formed in all the samples where the current density reaches a constant value over a definite potential range. In addition, as the current density increases, the breakdown of the passive layer is observed in the Tafel curves.

According to the ASTM G102-89 standard [206], the corrosion rate C_R (in mm/year) can be calculated as:

$$C_R = \frac{K * i_{corr} * E_W}{\rho} \quad \text{.....(5.1)}$$

where K = 3.27 × 10^{-3} mm.g/μA.cm.yr, i_{corr} = corrosion current density at E_{corr} (μA/cm^2), E_W = equivalent weight of Ti-6Al-4V alloy (26.97 gm-equivalent), ρ = density of Ti-6Al-4V alloy (4.41 g/cm^3). The value of the corrosion rate is mentioned in Table 5.1. The HT sample shows a lower corrosion rate (0.001164 mm/year) than the AB sample (0.003130 mm/year).

If the potential is increased, both the AB and HT samples achieve the corresponding steady passive current densities. Partial stabilisation of the passive current density implies formation of passive film. In addition, a slight change in current density with respect to potential is also observed at around 626 mV, which may be related to the creation and re-passivation of micro-sized pits, also known as "metastable pits". This is due to solution oxidation (evolution of oxygen), which occurs through transferring electrons to the oxides.

The HT sample showed a lesser i_{corr} value (1.319 × 10^{-7} A/cm^2) as compared to the i_{corr} value (3.547 × 10^{-7} A/cm^2) of the AB sample. However, there is no significant enhancement in the E_{corr} value (–0.291 V) of the HT sample compared to the AB sample (–0.356 V). Additionally, the i_{corr} value of HT samples in this study is lower than that discussed in other Ringer's solution studies [128, 207]. In those studies, HT reduced i_{corr} value, while there was no effect on E_{corr} value. The sample microstructure has been attributed to this type of behaviour (Figure 3.5). The microstructure after HT revealed increase of β phase that enhances corrosion resistance of the samples.

After the corrosion tests, the corroded samples were examined under SEM to observe initiation of pits; the AB samples accomplished notable pitting. However, after HT at 800 °C, this localized corrosion becomes less severe or is almost eliminated. The HT AM samples corrode uniformly, as shown in Figure 5.7 (b). This observation is supported by the Tafel plots (Table 5.1) and is similar to earlier observations [128, 134, 207, 208]. The AB sample is found more prone to corrosion than the HT sample.

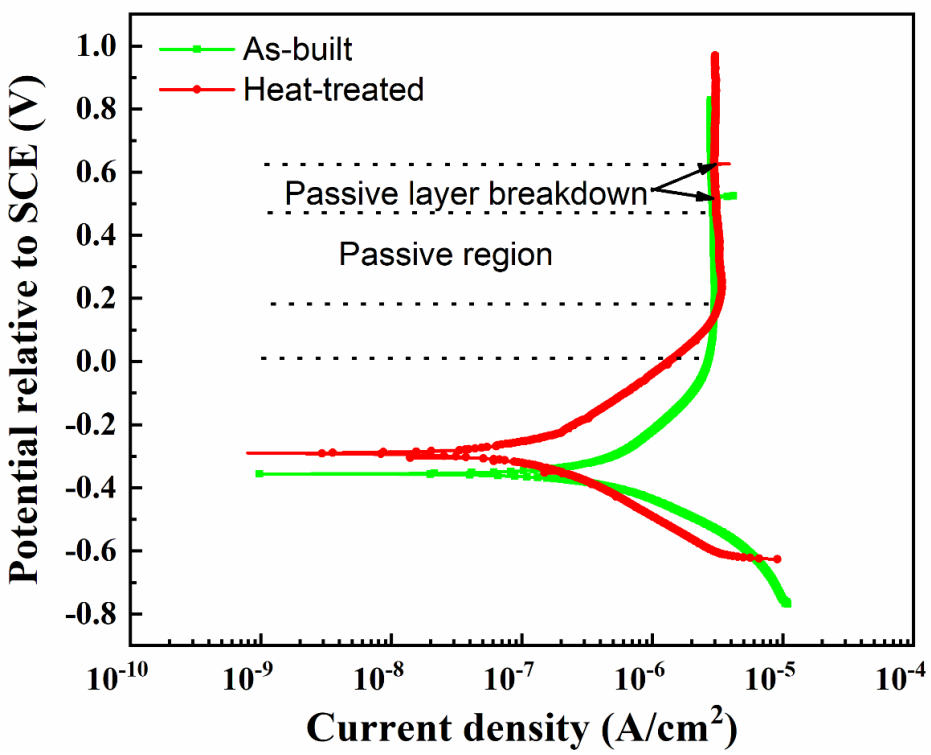

Figure 5.1 Tafel plots of AB and HT samples in Ringer's solution

Table 5.1 Electrochemical properties derived from Tafel curves

Sample	E_{corr} (V)	i_{corr} (μA/cm^2)	β_a (mV/decade)	β_c (mV/decade)	Corrosion rate (mm/year)
AB	–0.356 ± 0.02	0.3547 ± 0.03	311.12 ± 1.16	–186.24± 0.24	0.003130
HT	–0.291 ± 0.01	0.1319 ± 0.011	301.5 ± 0.85	–234.8 ± 0.49	0.001164

For confirmation of the potentiodynamic polarization results, EIS measurements were conducted to evaluate corrosion behaviour of the AM samples by representing the Nyquist and Bode plots and their related equivalent circuits. Figure 5.2 and Figure 5.3 represent the Nyquist plot, between real part (Z') and imaginary part (Z'') of impedance, and Bode plots with respect to different frequencies, respectively. In both conditions, the Nyquist plots are nearly semi-circular (Figure 5.2), which is characteristic of a capacitor [135, 209].

A larger radius of the Nyquist plot's curve indicates better corrosion resistance [134]. Figure 5.2 shows this behaviour; the HT samples exhibit larger arc curvature as compared to AB samples. The top of the semicircle in the AB sample has near 100 kΩ resistance. The semicircle for the HT sample reached approximately 150 kΩ resistance in the intermediate region and approximately 300 kΩ resistance at the end of the curve on the horizontal axis. This showed a greater R_p value for the HT sample, which is verified by measured EIS data as shown in Table 5.2.

The Bode plot presents the trend of the system's capacitive, inductive, and resistive behaviour at various frequencies. Figure 5.3 (a) is drawn between the magnitudes of impedance spectra and frequency. Figure 5.3 (b) is drawn between the phase angle and frequency. A logarithmic frequency axis is used to plot the frequency. The impedance spectra of Bode plots of AB and HT samples showed two distinct regions, as shown in Figure 5.3 (a).

For the high-frequency zone, the $\log|z|$ value is shifted towards the constant values while the values of the phase angle (Figure 5.3 (b)) approach zero with respect to the logarithmic scale of frequency. This highlights solution resistance response, and it shows that all the samples have good solution resistance. The spectra showed almost linear

slopes of −1 for the low and medium frequency zones (1 kHz − 100 mHz). It is a typical behaviour of capacitance in surface film of the samples [210].

In the low frequency zone, the phase angles of the sample decreased significantly and approached the lower sides due to involvement of the impedance to the surface film resistance. The value of phase angle reaches approximately 85° at lower frequencies, indicating that a passive layer (i.e., a protective film) has been developed on the AB and HT samples in Ringer's solution.

In the low frequency impedance, the plots of the samples revealed an improvement in the phase angle with time. In the intermediate frequency region, the phase angle increases with time. This prompted creation and development of passive protection films. In addition, the low frequency impedance in the HT sample resulted in a significant increase in the phase angle, which suggests positive considerations for creation of the passive protective films.

The measured EIS data is modelled using the CPE circuit illustrated in Figure 5.4. The associated parameters for the equivalent circuit have been shown in Table 5.2. Due to surface non-uniformity, impurities, defects such as pores, and the formation of a porous layer, a CPE (indicating a change from the behavior of an ideal capacitor) has been used to replace pure capacitance [211]. The impedance of the CPE is

$$\boldsymbol{Z_{CPE} = \frac{1}{Q_o}(j\omega)^{-n}} \quad \text{.....(5.2)}$$

where Q_o represents the equivalent capacitance ($F.cm^2.s^{(n-1)}$), j denotes imaginary unit number, ω is angular frequency, F represents Faraday constant, and n represents coefficient of diffusion that lies between $-1 \leq n \leq 1$. Here, $n = -1$ belongs to pure inductance, $n = 0$ represents an ideal resistance, and $n = 1$ represents an ideal

capacitance. For the AB and HT samples, the equivalent circuit offered the best fitting based on Nyquist plot, Bode plots, and lowest Chi-square values. The fitting confidence has been calculated using the Chi-square value. A Chi-square value (χ^2) represents the standard deviation between the obtained and fitting values. In general, the lower the χ^2 value, the more accurate is the suggested model shown in Figure 5.4 [212].

In this circuit, R_s and R_p refer to resistance of Ringer's solution and the passive layer resistance between the solution and the metal, respectively. CPE_1 represents capacitive property of the passive region, CPE_2 and R_{ct} indicate capacitive properties and resistance to charge transfer of the electrochemical double region. In accordance with these findings, all samples are governed by a single process that is primarily controlled by charge transfer in the passive film. These findings are consistent with the literature [134, 135]. Consistent reading of the R_s values, independent of sample type or test setup, suggests that tests are highly reproducible. A closer look at the EIS data (Table 5.2) showed that the HT sample displayed both R_s (69.98 Ω.cm^2) and R_p (284750 Ω.cm^2) values greater than those of the AB sample.

The Nyquist plot does not exhibit capacitive behaviour because the value of parameter n_2 (CPE component) from the modelled circuit is not close to unity, as also reported by other researchers [123, 134]. This indicated that the oxide film that forms on the sample surface of the alloy is not conductive, protecting it from corrosion. The charge-transfer resistance values for the AB and HT samples are 310130 Ω.cm^2 and 98096 Ω.cm^2, respectively. The large value of R_{ct} suggests a thicker and more balanced oxide in the HT samples, which inhibits dissolution. As a result, heat treatment promotes the oxide layer development and prevents the samples against corrosion [134]. These findings are also consistent with those obtained from Tafel plot.

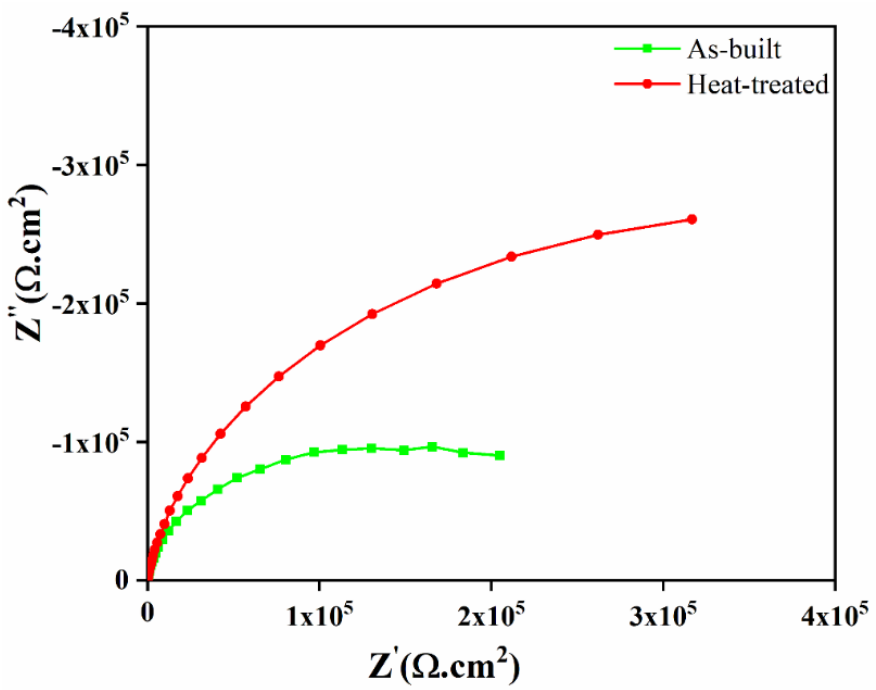

Figure 5.2 Nyquist plots of AB and HT AM samples in Ringer's solution

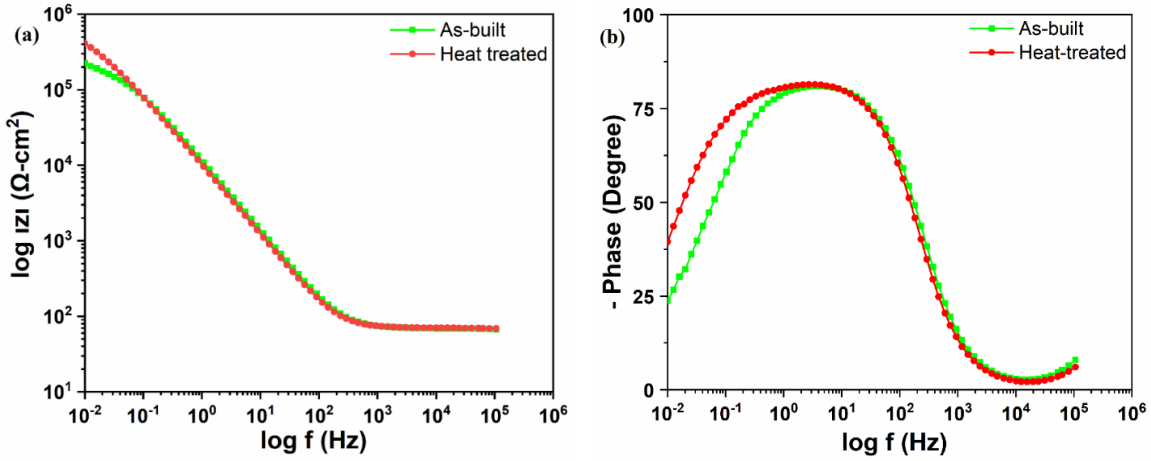

Figure 5.3 Bode plots of AM samples; (a) impedance spectra obtained in Ringer's solution and (b) trends corresponding to the bode plots with respect to phase angle

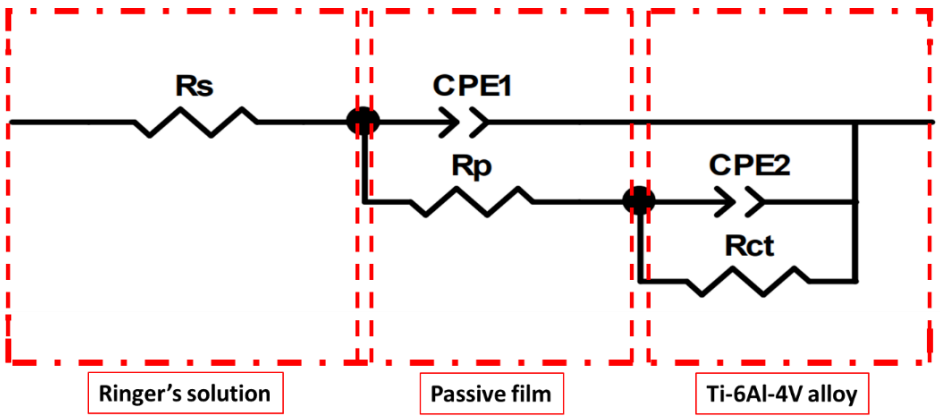

Figure 5.4 Equivalent circuit models for fitting and simulating the impedance spectra

Table 5.2 Electrochemical parameters of equivalent electric circuit model of corrosion samples and goodness of fit (χ^2) in Ringer's solution

Samples	R_s	R_p	CPE_1		R_{ct}	CPE_2		χ^2
	(Ωcm^2)	(Ωcm^2)	Q_1 ($\Omega cm^{-2}s^n$)	n_1	(Ωcm^2)	Q_2 ($\Omega cm^{-2}s^n$)	n_2	(10^{-2})
AB	69.08	174490	1.5682×10^{-5}	0.92444	98096	6.9294×10^{-5}	0.85957	0.27
HT	69.98	284750	1.7616×10^{-5}	0.92607	310130	7.7797×10^{-6}	0.73444	0.19

5.1.2 XPS analysis of the surface layer of AB and HT samples

Figure 5.5 presents XPS spectra of the surface layer of the AB and HT samples. Numerous elements, including Ti, Al, V, Fe, C, O, etc., have been found in the AM Ti-6Al-4V surfaces. The two main elements in titanium oxide (TiO_2) are Ti and O, and these have been identified in all the samples. C and N have emerged from the air or Ringer's solution [132]. All the surfaces of the sample are also made of Al_2O_3, but the Ti-6Al-4V alloy only contains 6% aluminium. The vanadium content is substantially lower (4%), making it challenging to fit the V2p region more precisely. As a consequence, the Ti2p and Al2p spectra are the main focus of the XPS analysis of the alloy's surface.

Figure 5.6 (a) depicts the high resolution XPS spectra of the Ti2p region. According to Figure 5.6 (a), the Ti2p photoemission signal separates into two peaks. The first one is related to Ti2p3/2 (IV) with 458.3 eV energy, while the second one is allotted to Ti2p1/2 (IV) at the energy of 465 eV, of the samples. The presence of the Ti (IV) element indicates that TiO_2 has the component of the oxide film [135].

Table 5.3 displays the Ti2p, Al2p, C1s, and O1s peak binding energies, full-width-at-half-maximum (FWHM), and atomic % of AB and HT samples. Atomic percentage of Ti, Al, oxygen in the surface layer increased considerably in the HT samples and the oxide layer thickness also increased, which is necessary for the alloy's ability to resist corrosion (Table 5.3). Hence, a stable oxide layer of TiO_2 is created on the surface of the samples [89]. The HT sample demonstrated better passive behaviour than the AB sample because of more enduring oxide films. The microstructure of AB samples contained martensitic α′ phases and the microstructure of HT sample consisted of α and β phases. It is believed that low corrosion resistance of the AB sample is due to martensitic α′ phase [134].

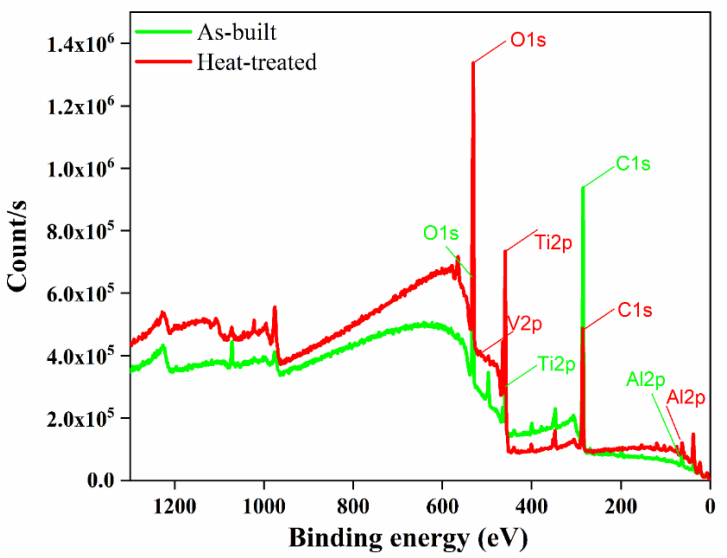

Figure 5.5 The XPS of the surface layer of corrosion samples of AB and HT additively manufactured samples in Ringer's solution

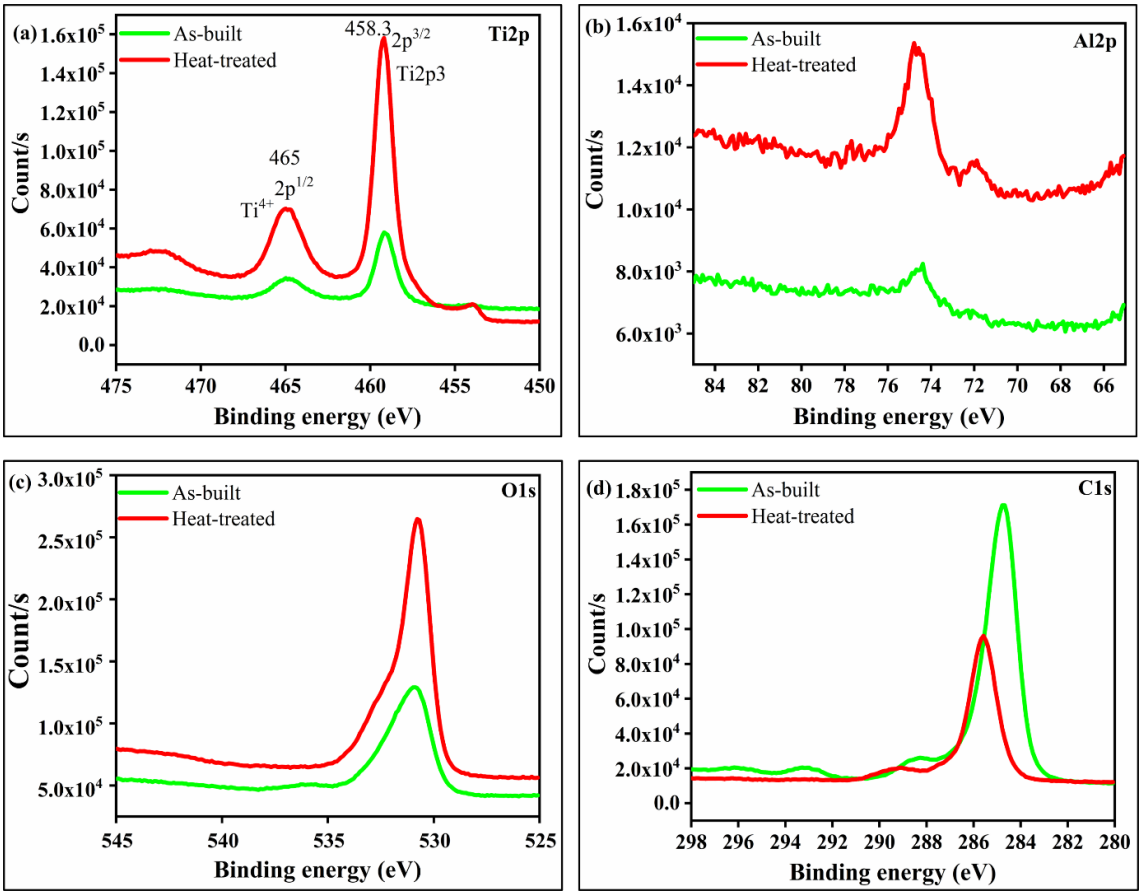

Figure 5.6 XPS of (a) Ti2p, (b) Al2p, (c) O1s, and (d) C1s regions for AB and HT AM samples exposed to Ringer's solution

Table 5.3 Ti2p, Al2p, C1s, and O1s peak binding energy, FWHM, and atomic % of AB and HT samples

Sample	Peak binding energy, $Ti2p^{3/2}$ (eV)				FWHM (eV)				Atomic %			
	Ti2p	Al2p	C1s	O1s	Ti2p	Al2p	C1s	O1s	Ti2p	Al2p	C1s	O1s
AB	459.14	74.59	285.2	531.48	2.81	1.95	2.76	3.33	3.23	0.66	75.23	20.88
HT	459.17	74.79	285.93	531.24	2.80	1.67	2.69	3.21	13.81	2.83	42	41.36

5.1.3 Microstructure analysis of the samples after corrosion test

Figure 5.7 shows the surface features of the AB and HT samples following EIS testing in Ringer's solution. The weight percentage of various elements present on the surface of AB and HT corroded samples has been depicted in Figure 5.7. The surface of the AB sample has numerous pits, whereas the surface of the HT samples has only a few pits. The

non-equilibrium phase present in AB samples is the main reason of the pits, as a consequence of which a less protective passive layer is formed. In terms of corrosion, the AB samples naturally have a greater state of energy.

Corrosion cells can form as a result of the increased energy, and stressed regions are regarded as anodic zones, allowing them to dissolve more easily. The presence of the β phase in equilibrium in the structures after heat treatment results in high corrosion resistance and high protective passive layer formation, which means that elimination of the needle-shaped strained martensitic phase improved the corrosion performance in the samples [13]. The oxide layers generated on the samples are not electrically conductive; hence the alloy will be protected in Ringer's solution. The main cause of the decrease in corrosion rate and the rise in E_{corr} value is the homogenization process during HT.

According to the aforesaid discussion, it is clear that, Ti-6Al-4V with β phase sample is more resistant to corrosion than Ti-6Al-4V with α phase sample. This behaviour is caused by the more stable oxide film that forms on the Ti-6Al-4V with β-phase samples [134]. This is consistent with the findings from Tafel plots and XPS analysis of different samples. The surface defects are due to corrosion pits in the samples, as depicted in Figure 5.7 (a). In general, there are three stages (passive breakdown, pit initiation, and pit propagation) for the occurrence of pitting corrosion. Due to pitting, passive film breakdown and penetration are observed in AM samples.

For the HT sample, flake type corrosion products are observed, as depicted in Figure 5.7 (b). The occurrence of pitting corrosion in metals and alloys is caused by physical variability on the metal surface due to inclusions, mechanical damage, and dislocations, as reported by other researchers [128, 135]. Additionally, the surface roughness led to development of cracks and pits in the interfacial zone. As a result, this deterioration of the

passive films can make it easy for corrosive solutions to enter inside the Ti-6Al-4V alloy [132, 207].

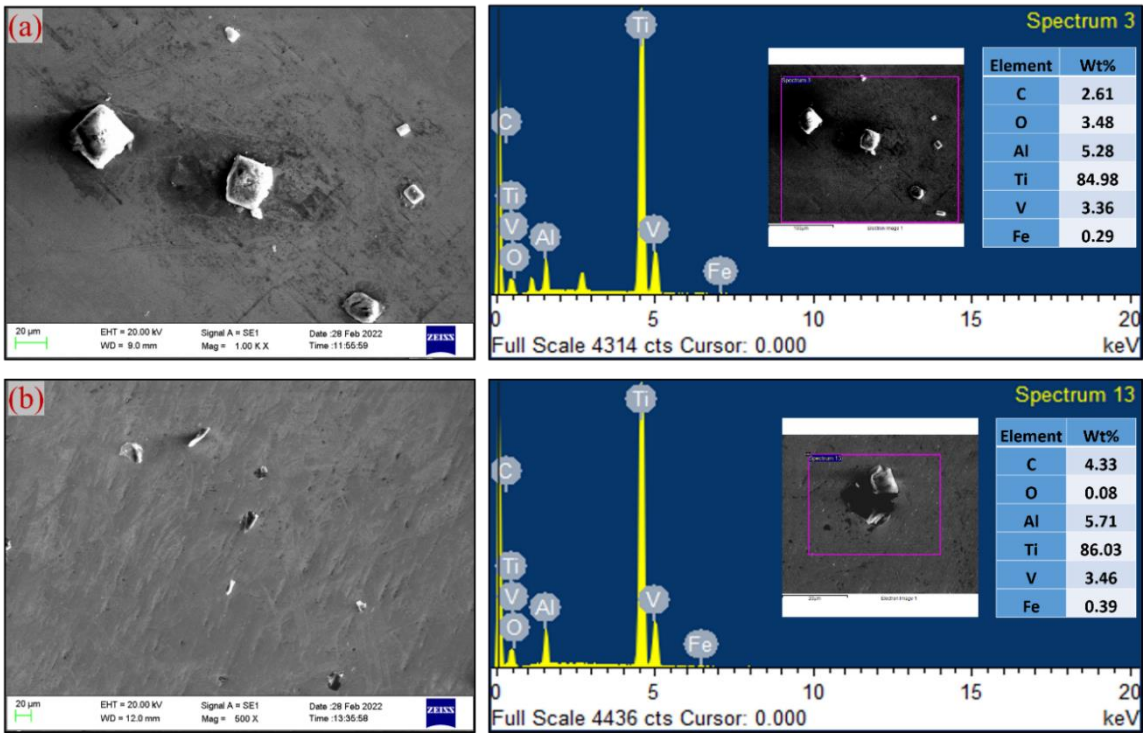

Figure 5.7 SEM with EDS of corroded regions of (a) AB and (b) HT additively manufactured samples after EIS testing in Ringer's solution

5.1.4 Corrosion rate measurement of conventional and AM samples in different orientations

The Tafel plots of the as-built and heat-treated conventional and AM samples in different orientations are presented in Figure 5.8. The electrochemical properties such as corrosion potential (E_{corr}), current density (i_{corr}), and corrosion rate (mm/year) obtained from Tafel curves for conventional and AM samples in different orientations are shown in Table 5.4.

Figure 5.8 (a) presents the Tafel plots of as-built conventional and AM samples in Ringer's solution. From the plots, it is noticed that the as-built conventional and AM 45° oriented samples have shown passive region where constant current density approaches over a certain potential range. The E_{corr} value of as-built conventional (-0.091± 0.02 V) and AM 0° oriented (-0.088± 0.01 V) samples is comparable but the Tafel curve of the conventional sample has shifted towards lower current density than that of the AM 0° oriented sample.

The E_{corr} and i_{corr} values for the AM AB-45° and AB-90°oriented samples are -0.119 ± 0.04 V and 0.034 ± 0.02 μA/cm^2 and -0.095 ± 0.05 V and 0.0267 ± 0.02 μA/cm^2, respectively. The corrosion current for AM 0° oriented samples is significantly higher than that of AM 45° and 90° oriented samples. In general, a lower value of corrosion current in the Ringer's solution indicates that the Ti-6Al-4V samples can be easily passivated and have strong corrosion resistance [213].

The corrosion rate (mm/year) is calculated according to the ASTM G102-89 [206] standard using equation (5.1) where the value of density for each orientation is taken from our previous publication [213]. It is concluded that the decreasing order of corrosion rate is as follows: AM AB-0° > AM AB-45° > Conv_AB > AM AB-90°. Thus, it is observed that corrosion rate decreases when build orientation increases from 0° to 90° in as-built condition. For the same energy input, AM 0° oriented samples experience higher heat dissipation through the already deposited metallic layer than AM 45° and 90° oriented samples.

For AM 45° oriented samples, more powder particles exist below the new solidified area. Therefore, thermal gradient between new layer and previous layer reduces due to poor thermal conductivity of the powder particles compared to the corresponding solid

component in the supporting area and lowers the degree of heat transfer. From the above statement, it can be concluded that the AM 0° oriented samples exhibit more degree of heat transfer, because of this, AM 0° oriented samples showed more fine acicular martensitic structure in comparison to AM 45° and 90° oriented samples. This could be the reason of high corrosion rate in AM AB-0° samples in comparison to AB-45° and AB-90° samples.

The Tafel plots of heat-treated (HT) conventional and AM samples in different orientations are shown in Figure 5.8 (b). From the plots, it is noticed that all Tafel curves of HT samples have shown passive region. The corrosion potential and corrosion current for AM HT build in different orientations are as follows: 0° (E_{corr} = -0.179 ± 0.06 V and i_{corr} = 0.028 ± 0.01 μA/cm^2), 45° (E_{corr} = -0.182 ± 0.02 V and i_{corr} = 0.0271 ± 0.06 μA/cm^2), and 90° (E_{corr} = -0.238 ± 0.07 V and i_{corr} = 0.0267 ± 0.03 μA/cm^2). The corrosion current of AM HT-0° samples is higher than that of AM HT-45° and HT-90° samples. Therefore, the corrosion rate of AM HT-90° samples is lower in comparison to that of AM HT-0° and AM HT-45° samples.

The conventional HT samples (i_{corr} = 0.065 ± 0.08 μA/cm^2) observed a higher corrosion current than the AM HT samples. The order of decreasing corrosion rate (mm/year) is as follows: Conv_HT (0.000573) > AM HT-0° (0.000247) > AM HT-45° (0.000239) > AM AHT-90° (0.000234). So, it is concluded that the corrosion rate slightly decreases when the build orientation increases from 0° to 90° in heat-treated condition. In other way, the AM HT samples in different orientations exhibit approximately equivalent corrosion rates, so we can conclude that the heat treatment reduces the effect of anisotropy on the corrosion rate of additively manufactured Ti-6Al-4V samples in Ringer's solution.

By comparing the corrosion current between the as-built and heat-treated samples shown in Table 5.4 and from the plots, it is noticed that the Tafel curves of AM HT samples have shifted towards lower current density compared to that of AM AB and conventional samples. Means, the AM AB sample is more susceptible to corrosion than the AM and conventional HT sample. Due to high cooling rate during the AM process, the as-built sample exhibited fine acicular α′ martensitic structure [15].

After heat treatment of AM Ti-6Al-4V samples, the β phase evolves along the grain boundaries of the α′ phase. The vanadium atoms come out of the supersaturated α′ solid solution; as a result, vanadium is enhanced locally, β phase forms along the grain boundaries, and α′ is converted into α phase. Therefore, the microstructure after HT exhibited presence of β phase, as a result, improved the corrosion resistance of AM Ti-6Al-4V samples.

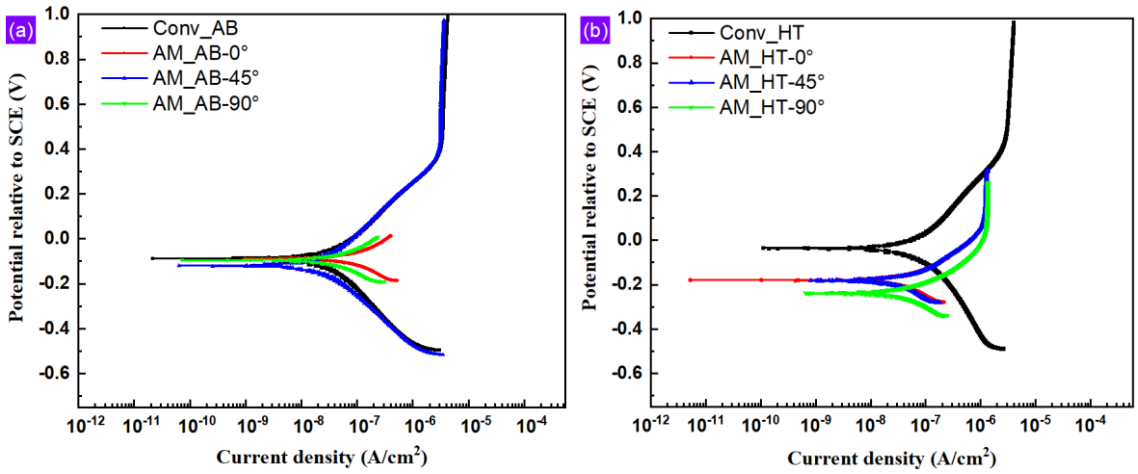

Figure 5.8 Combined Tafel plots for conventional and AM Ti-6Al-4V samples in different orientations: (a) as-built and (b) heat-treated samples

Table 5.4 Electrochemical properties obtained from Tafel curves for conventional and AM samples in different orientations

Sample	E_{corr} (V)	i_{corr} (μA/cm²)	β_a (mV/decade)	β_c (mV/decade)	Corrosion rate (mm/year)
Conv_AB	-0.091± 0.02	0.030± 0.001	221.99± 1.89	218.18± 0.85	0.000264
AM_AB-0°	-0.088± 0.01	0.089± 0.09	108.10± 1.09	128.46± 0.24	0.000785
AM_AB-45°	-0.119± 0.04	0.034± 0.02	255.13± 0.84	249.1± 1.17	0.000300

AM_AB-90°	-0.095± 0.05	0.0267± 0.02	81.78± 0.98	79.88± 0.67	0.000239
Conv_HT	-0.033± 0.01	0.065± 0.08	258.30± 1.95	222.59± 1.5	0.000573
AM_HT-0°	-0.179± 0.06	0.028± 0.01	84.70± 0.23	108.37± 1.2	0.000247
AM_HT-45°	-0.182± 0.02	0.0271± 0.06	108.53± 1.06	116.62± 0.96	0.000239
AM_HT-90°	-0.238± 0.07	0.0267± 0.03	91.55± 0.95	79.40± 0.87	0.000234

5.1.5 Electrochemical impedance spectroscopy (EIS) of samples in different orientations

EIS analysis was conducted on conventional and AM as-built and heat-treated samples to examine the corrosion behaviour in Ringer's solution and based on that Nyquist and Bode plots are presented in Figure 5.9 – Figure 5.11. Figure 5.9 (a) and (b) present the Nyquist plots for as-built and heat-treated conventional as well as AM Ti-6Al-4V samples in different orientations, respectively.

In AM as-built samples, it is observed that the arc curvature increases when the build orientation increases from 0° to 45° and then decreases when the build orientation again increases from 45° to 90°. The arc curvature of conventional as-built samples was found between the arc curvatures of AM 45° and 90° oriented as-built samples. Therefore, the decreasing order of arc curvature for as-built samples is as follows: AM AB-45° > Conv_AB > AM AB-90° > AM AB-0°. It is well known that a bigger arc radius of Nyquist curve represents the better corrosion resistance [134].

So, according to Nyquist curve, the AM 45° oriented as-built samples showed better corrosion resistance than AM 0° and 90° oriented as-built samples. The AM AB-0° oriented samples experienced lower corrosion resistance due to finer acicular martensitic phase than AM 45° and 90° samples.

In AM heat-treated samples, it is noticed that the arc curvature of 0° oriented samples lies between the arc curvatures of 45° and 90° oriented samples. Therefore, the arc curvature increases as build orientation increases from 0° to 45° and then decreases when the build orientation again increases from 45° to 90° in the heat-treated samples. Therefore, the decreasing order of arc curvature for heat-treated samples is as follows: AM HT-45° > AM HT-0° > AM HT-90° > Conv_HT.

The arc curvature of conventional heat-treated samples was found lower than that of the AM heat-treated samples. Therefore, it is concluded that the AM samples show better corrosion resistance than conventional samples after heat treatment. Also, the heat-treated samples show large arc curvature than the as-built samples except the AM 45° and conventional samples because the microstructure after HT exhibited the presence of β phase, as a result, there was improved the corrosion resistance of AM Ti-6Al-4V samples.

For AM 45° samples, the arc curvature of heat-treated samples was found to be lower than that of the as-built samples, because the distribution of grain size in 45° oriented samples is still in the finer grain side and has not converted significantly. The above mentioned results have been thoroughly discussed in our previous publication [174].

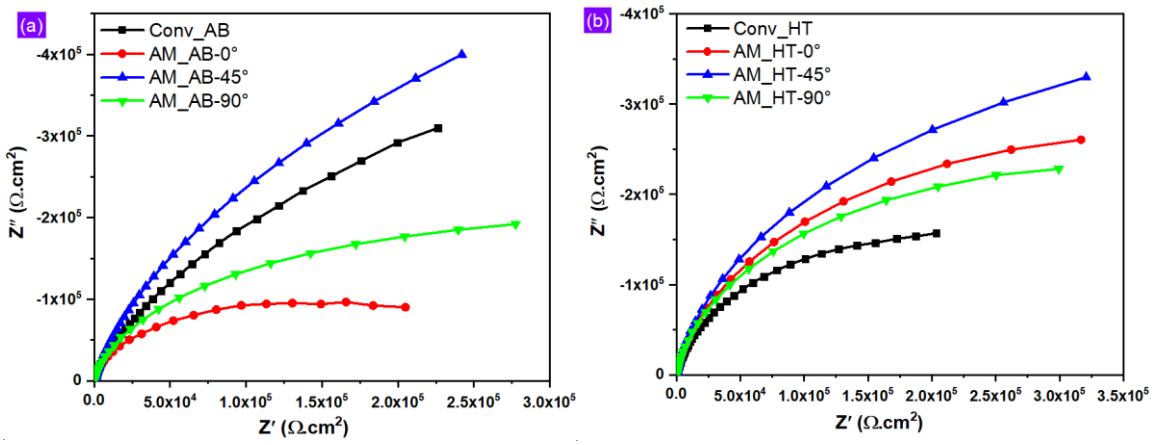

Figure 5.9 Combined Nyquist plots for conventional and AM Ti-6Al-4V samples of (a) as-built and (b) heat-treated samples

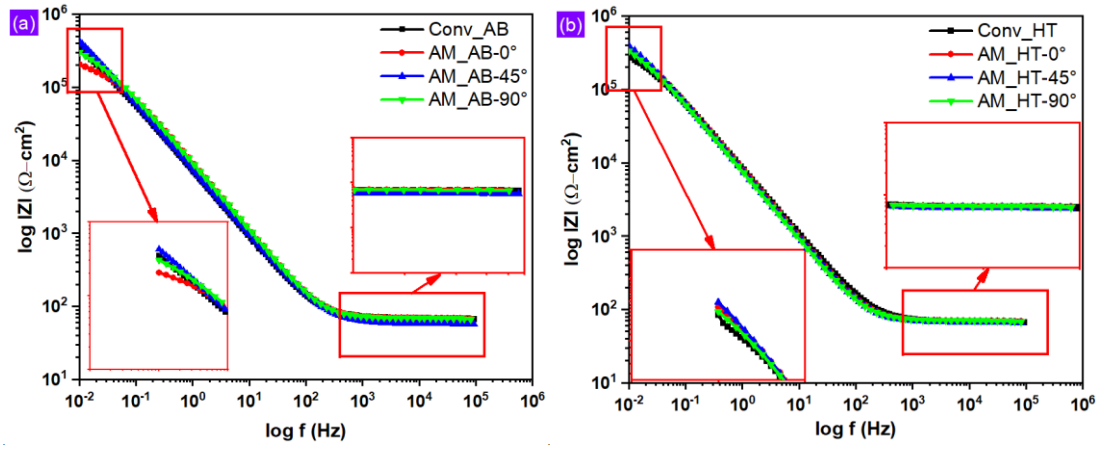

Figure 5.10 Impedance spectra obtained from Bode plots in Ringer's solution for conventional and AM samples: (a) as-built and (b) heat-treated samples

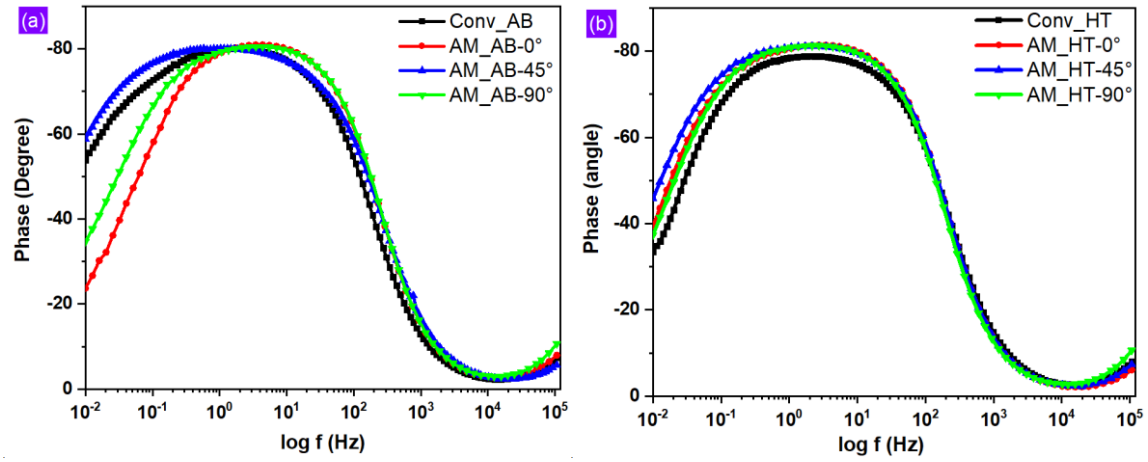

Figure 5.11 Trends corresponding to the Bode plots with respect to phase angle for the conventional and AM samples: (a) as-built and (b) heat-treated samples

Figure 5.10 (a) presents the impedance spectra from Bode plots of conventional and AM as-built samples, whereas, Figure 5.10 (b) presents the impedance spectra from Bode plots of the conventional and AM heat-treated samples in different orientations. The Bode curve presents the trend of resistive, capacitive, and inductive behaviours of the system at different frequencies.

Figure 5.11 (a) and (b) present the Bode plots with respect to phase angle for conventional as well as the AM as-built and heat-treated samples, respectively, in different orientations. The impedance spectra of Bode plots showed two distinct zones, the first is high frequency zone and the second is low frequency zone. The value of $log|z|$ in high frequency zone has reached to the constant values while the phase angle approaches to zero with respect to frequency plotted on logarithmic scale (Figure 5.11 (a) and (b)). This trend shows that the conventional as well as AM as-built and heat-treated samples have good solution resistance.

Also, the impedance spectra of all the samples show almost constant linear slope in the medium frequency zone and this behaviour exhibits the existence of capacitance in the surface films of all the samples [210]. The phase angles of all the samples decreased significantly and approached the lower sides in the low frequency zone due to the involvement of impedance to the surface film resistance. The variation of phase angles in the as-built samples is more in comparison with that of the heat-treated samples.

The AM AB-45° samples experience higher phase angle in comparison with the AM AB-0° and AB-90°, as a result these samples exhibit more solution resistance. The lowest phase angle was found in the AM AB-0°, followed by AM AB-90° and then conventional as-built samples. At lower frequencies, the phase angle reaches around 80°, indicating that a passive layer or protective film is formed on the conventional and additively manufactured samples in Ringer's solution.

The phase angle increases with time in the intermediate frequency range; hence this caused the formation of protective passive films. Furthermore, the conventional and AM heat-treated samples have nearly the same phase angle at low frequency.

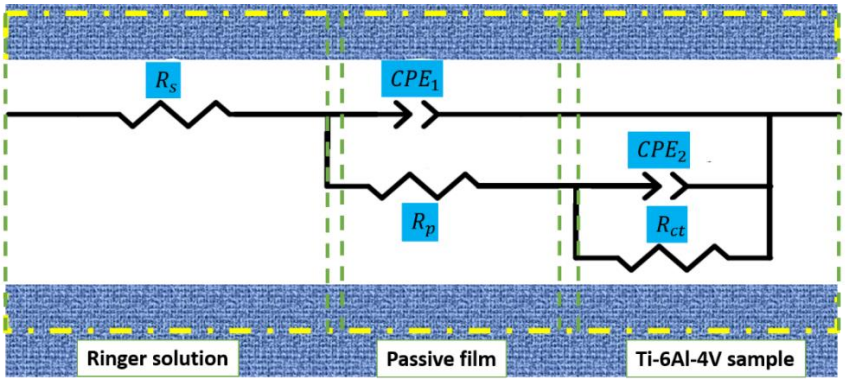

Figure 5.12 Equivalent circuit models for fitting and simulating the impedance spectra

Table 5.5 Electrochemical parameters of equivalent electric circuit model of corrosion samples and goodness of fit

Samples	R_s ($\Omega.cm^2$)	R_p ($\Omega.cm^2$)	CPE_1		R_{ct} ($\Omega.cm^2$)	CPE_2		χ^2 (10^{-2})
			Q_1 ($\Omega cm^{-2}s^n$)	n_1		Q_2 ($\Omega cm^{-2}s^n$)	n_2	
Conv_AB	69.42	448680	2.3299×10^{-5}	0.90259	297320	2.9413×10^{-5}	1.112	0.26041
AM_AB-0°	69.03	92134	2.3038×10^{-5}	0.93229	175680	4.9649×10^{-5}	0.90679	0.26812
AM_AB-45°	57.96	1567	2.109×10^{-5}	0.89644	1117900	1.4103×10^{-6}	0.92764	0.13146
AM_AB-90°	68.33	229930	6.117×10^{-5}	0.94901	10393	2.135×10^{-5}	0.91348	0.48088
Conv_HT	69.13	375930	2.0891×10^{-5}	0.89438	363770	2.1511×10^{-5}	0.88696	0.46446
AM_HT-0°	69.89	35906	6.8043×10^{-5}	0.88987	528010	2.3798×10^{-5}	0.94032	0.18979
AM_HT-45°	67.09	37574	8.5606×10^{-5}	0.86734	672540	2.3834×10^{-5}	0.94105	0.26953
AM_HT-90°	69.85	82367	4.3582×10^{-5}	0.88169	403720	3.2855×10^{-5}	0.9716	0.54399

Figure 5.12 presents the equivalent circuit model to fit and simulate impedance spectra of the EIS measurements. In this circuit, R_s is the solution resistance of Ringer's solution, R_p and R_{ct} present the film resistance and charge transfer resistance of the Ti-6Al-4V alloy in the solution. These values are very crucial for the corrosion of material. CPE_1 presents the capacitance of the passive film and CPE_2 presents the capacitance of the double layer.

Table 5.5 presents the related parameters used in this equivalent circuit model. In pace of ideal capacitor, a constant phase element, showing a different behaviour than an ideal capacitor, has been fitted due to surface non-uniformity, impurities, defects like pores, and porous layer formation. The CPE contains two parameters; Q presents the equivalent capacitance and n presents the coefficient of diffusion that ranges from -1 to 1. Ideal capacitance is represented by n = 1, ideal resistance is represented by n = 0, and pure inductance is represented by n = -1.

Based on the Nyquist plots, Bode plots, and lower Chi-square (χ^2) values, the equivalent circuit model provided the best fitting to obtain the actual values of different parameters. The standard deviation between the acquired and fitting values is represented by a Chi-square value and it has been utilized to compute the fitting confidence. Generally, lower value of Chi-square suggests that the model is more accurate and in this result, the Chi-square value was found to be less than 10^{-2} [212]. The lower value of Chi-square indicates that the equivalent circuit model used in this EIS measurement is accurate. These outcomes are in line with previous findings [134, 135].

The corrosion tests are highly reproducible irrespective of sample types because of the consistent readings of solution resistance. It is observed from the EIS data shown in Table 5.5 that the AM HT samples had higher R_s values than the AM AB samples, but for conventional samples, the AB samples had higher R_s values than the HT sample. For as-built conventional and AM samples, the order of decreasing R_s values are as follows: Conv_AB (69.42 Ω.cm^2) > AM AB-0° (69.03 Ω.cm^2) > AM AB-90° (68.33 Ω.cm^2) > AM AB-45° (57.96 Ω.cm^2) and the order of decreasing R_{ct} values are as follows: AM AB-45° (1117900 Ω.cm^2) > Conv_AB (297320 Ω.cm^2) > AM AB-0° (175680 Ω.cm^2) > AM AB-90° (1-393 Ω.cm^2).

Also, the Nyquist plot does not indicate capacitive response because the value of CPE parameter i.e., n_2 is not equal to unity. This indicates that the oxide films formed on the sample surface are not conductive, thus protecting it from corrosion [123, 134]. For heat-treated conventional and AM samples, the order of decreasing R_s values are as follows: AM HT-0° (69.89 Ω.cm^2) > AM HT-90° (69.85 Ω.cm^2) > Conv_HT (69.13 Ω.cm^2) > AM HT-45° (67.09 Ω.cm^2) and the order of decreasing R_{ct} values are as follows: AM HT-45° (672540 Ω.cm^2) > AM HT-0° (528010 Ω.cm^2) > AM HT-90° (403720 Ω.cm^2) > Conv_HT (363770 Ω.cm^2). The high value of R_{ct} indicates that the AM HT-45° samples have a thicker and more balanced oxide, which avoids dissolution compared to AM HT-0° and AM HT-90°samples. The as-built conventional, AM AB-0°, and AM AB-90° samples had the smallest R_{ct} values than heat-treated conventional, AM HT-0°, and AM HT-90°, indicating that HT can promote the formation of oxide layers and protects the samples from corrosion [134].

With an increase in build orientation, the R_{ct} values of the as-built and heat-treated samples first increased and then decreased. The R_{ct} values of HT-45° samples were about 1.3 times and 1.7 times those of HT-0° and HT-90° samples, respectively. For AM 45° samples, the R_{ct} value of heat-treated samples was found to be lower than the as-built samples because the distribution of grain size is still on the finer side after the heat treatment. These findings are also consistent with the results of the Nyquist and Tafel plots.

5.1.6 XPS analysis of the surface layer of the conventional and AM samples in different orientations

XPS was performed on the surface layer of the as-built and heat-treated conventional and AM samples in different orientations to observe the elements including Ti, Al, V, Fe, C,

O, etc., available on the corroded surfaces. XPS was also used to analyse the oxide formation in corroded samples. Figure 5.13 presents XPS spectra of surface layer of the as-built and heat-treated conventional and AM samples in different orientations. Ti and O, the two primary elements of titanium oxide have been detected in each sample. Due to low percentage of Al (~ 6%) and V (~ 4%) in Ti-6Al-4V samples, it is difficult to precisely fit the V2p and Al2p regions. But some corroded samples showed the presence of aluminium oxide also.

Figure 5.13 (a) presents XPS spectra of the as-built conventional and AM samples in different orientations. The AM AB 45° corroded samples exhibited higher intensity and atomic % of O1s and Ti2p compared to that of the other build-oriented samples. For this reason, the AM 45° oriented as-built samples showed better corrosion resistance than AM 0° and 90° oriented as-built samples.

Figure 5.13 (b) presents XPS spectra of the heat-treated conventional and AM samples in different orientations. It is observed from Figure 5.13 (b) that, the AM HT 0° and HT 45° exhibit more intensity and atomic % of O1s and Ti2p compared to AM HT 90° samples. These findings confirm the results obtained from the Nyquist and Tafel plots. Consequently, the Ti2p and O1s spectra are the main focus of the XPS analysis of Ti-6Al-4V conventional and AM samples.

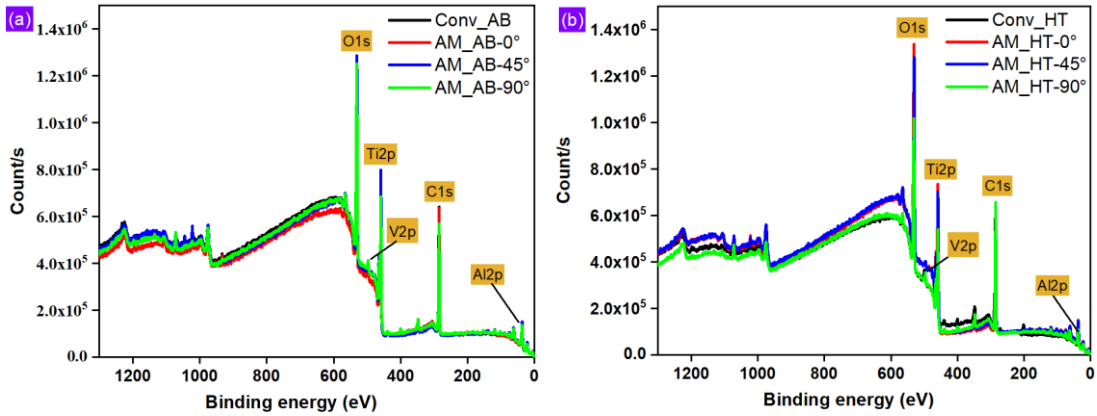

Figure 5.13 XPS spectra of surface layer of corrosion conventional and AM samples in different orientations: (a) as-built and (b) heat-treated samples

Figure 5.14 (a) presents the high resolution XPS spectra of the Ti2p region for the as-built samples, where two peaks were observed. The first one is associated with the binding energy of Ti2p3/2 (IV) at approx. 459 eV, and the second one is associated with the binding energy of Ti2p1/2 (IV) at approx. 465 eV. Figure 5.14 (b) presents the XPS spectra of the Al2p region with peak binding energy of approx. 75 eV.

Figure 5.14 (c) and (d) indicate the XPS spectra of O1s and C1s regions with peak binding energy at approx. 531 eV and 285 eV respectively. The presence of Ti (4+) element indicates that the TiO_2 is the oxide film component and protects surface layer of the Ti-6Al-4V samples. After heat treatment, Figure 5.15 (a) presents the high resolution XPS spectra of the Ti2p region, where two peaks were also observed. The first one is associated with the binding energy of Ti2p3/2 (IV) of approx. 458.6 eV for heat-treated conventional and AM 45° samples and at 459.2 eV for heat-treated AM 0° and AM 90° samples. The second one is associated with the binding energy of Ti2p1/2 (IV) at approx. 465 eV for all conventional and AM samples.

Figure 5.15 (b) presents XPS spectra of the Al2p region with peak binding energy of approx. 75 eV for all the samples. Figure 5.15 (c) and (d) indicate the XPS spectra of O1s and C1s regions with peak binding energy at approx. 530.1 eV for heat-treated conventional and AM 45° samples, and at 530.8 eV for the heat-treated AM 0° and AM 90° samples, and 285 eV respectively. These findings confirm that the heat-treated samples are more stable than the as-built samples, in line with the previous findings [134].

All the XPS fitting parameters like atomic percentage, full width at half maximum (FWHM), peak binding energies for Ti2p, Al2p, C1s, and O1s in conventional and AM as-built and heat-treated samples in different orientations are summarized in Table 5.6. The AM HT 0° samples showed a significant rise in the atomic percentage of Ti and O in the surface layer as well as an increase in the thickness of the oxide layer, which is required for the alloy to be corrosion-resistant. Hence, a persistent oxide layer of TiO_2 is formed on the surface of AM HT 0° samples. The heat-treated samples show more stable oxide layers over the surface because of the presence of β phase.

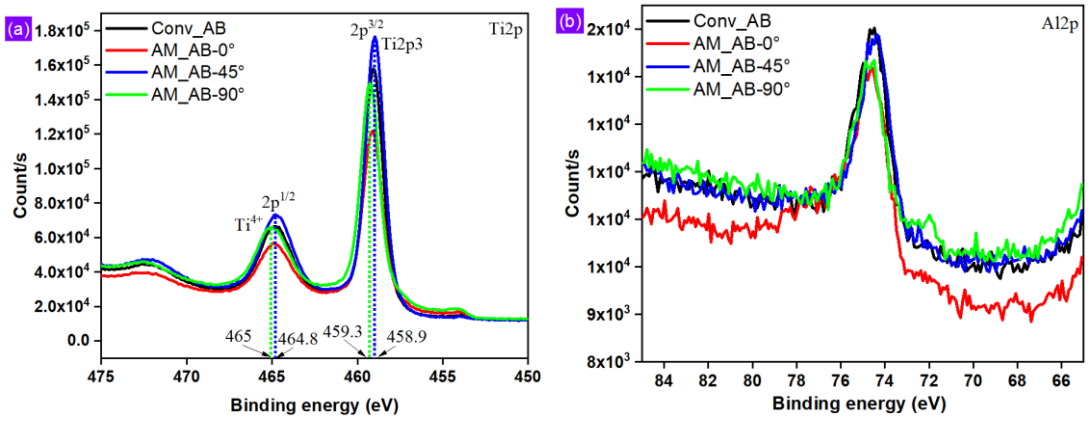

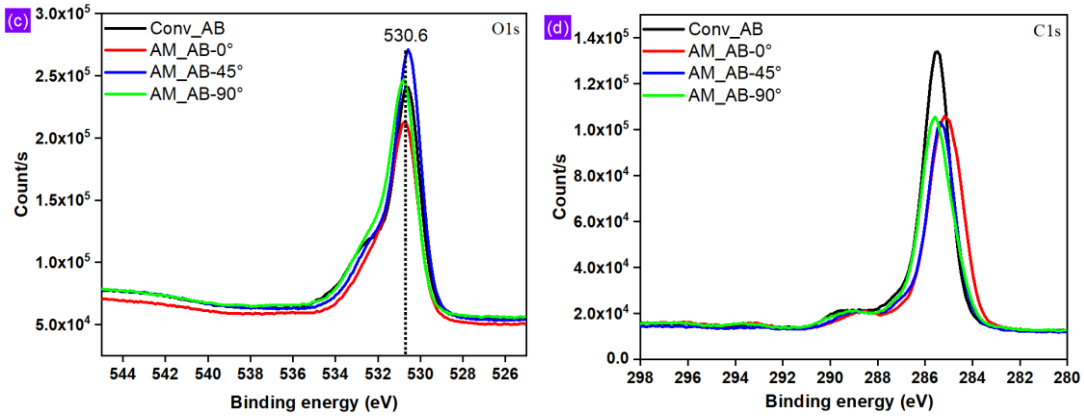

Figure 5.14 X-ray photon spectroscopy of as-built conventional and AM samples: (a) Ti2p, (b) Al2p, (c) O1s, and (d) C1s regions for different orientations

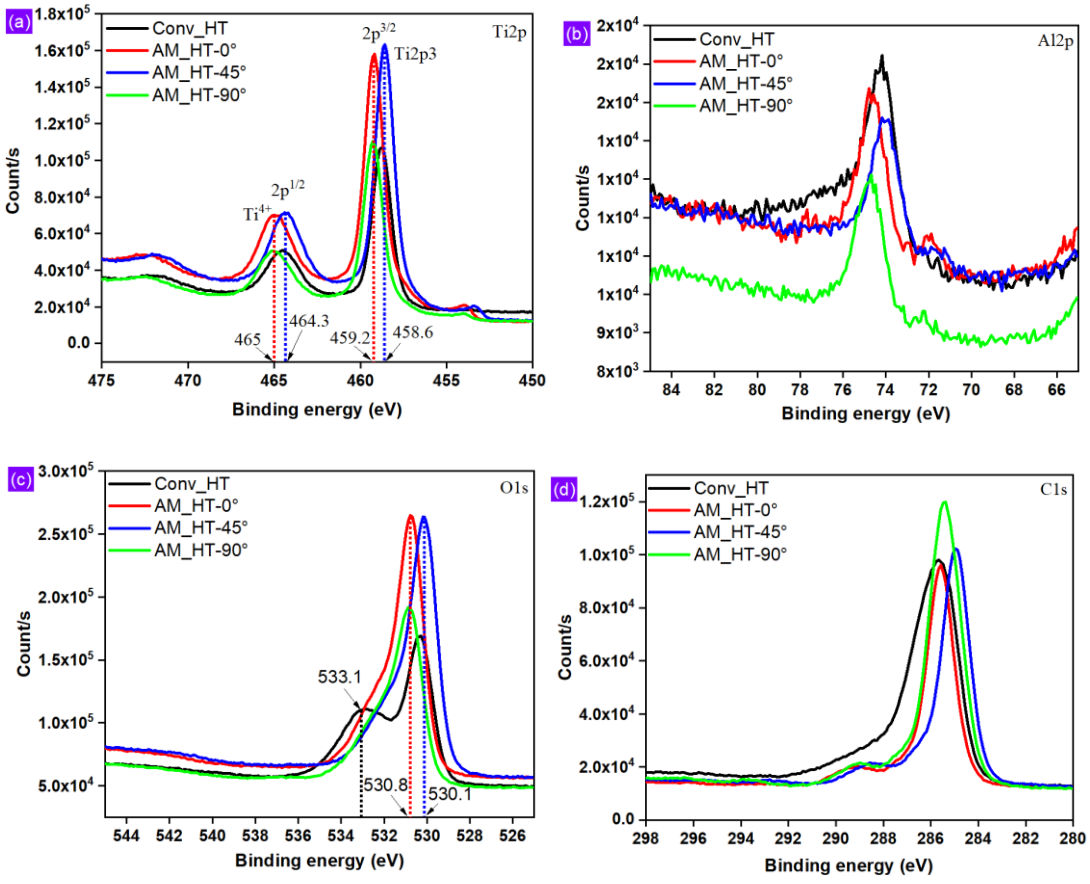

Figure 5.15 X-ray photon spectroscopy of heat-treated conventional and AM samples: (a) Ti2p, (b) Al2p, (c) O1s, and (d) C1s regions for different orientations

Table 5.6 Ti2p, Al2p, C1s, and O1s peak binding energy, FWHM, and atomic percent of conventional and AM as-built and heat-treated samples in different orientations

Sample	Peak binding energy, $Ti2p^{3/2}$ (eV)				FWHM (eV)				Atomic %			
	Ti2p	Al2p	C1s	O1s	Ti2p	Al2p	C1s	O1s	Ti2p	Al2p	C1s	O1s
Conv_AB	459.08	74.84	285.45	531.09	2.63	3.02	1.59	3.31	11.24	3.67	50.04	35.00
AM_AB-0°	459.10	75.06	285.22	531.13	2.80	3.06	2.75	3.18	10.45	3.30	52.37	33.88
AM_AB-45°	459.02	74.32	285.29	530.96	2.62	2.90	2.67	3.14	13.41	3.47	43.26	39.85
AM_AB-90°	459.16	74.89	285.41	531.22	2.75	3.11	1.75	3.25	11.6	2.63	48.48	37.27
Conv_HT	459.00	74.73	286.04	531.41	2.56	1.16	2.98	4.30	7.35	1.01	59.61	32.02
AM_HT-0°	459.17	74.79	285.93	531.24	2.8	1.67	2.69	3.21	13.81	2.83	42.00	41.36
AM_HT-45°	458.78	74.19	285.17	530.47	1.77	2.62	2.84	2.14	13.23	2.61	44.91	39.25
AM_HT-90°	459.14	74.88	285.43	531.32	2.72	2.54	1.66	3.46	9.10	2.84	57.33	30.74

5.1.7 Microstructural analysis of the samples after corrosion test in different orientations

The corroded conventional and AM samples fabricated in different orientations were examined by scanning electron microscope to observe the pit formation and differentiate the corrosion behaviour of the conventional and AM samples. Figure 5.16 presents surface morphology of the as-built conventional (Figure 5.16 (a) and (b)), AM 0° (Figure 5.16 (c) and (d)), AM 45° (Figure 5.16 (e) and (f)), and AM 90° (Figure 5.16 (g) and (h)) corroded samples.

Figure 5.16 also presents the weight percentage of different elements available on the corroded as-built conventional and AM samples. The AM AB 0° sample is found more prone to corrosion than AM AB 45° and AM AB 90° samples. As the build orientation increases from 0° to 90°, the weight percentage of oxygen initially increases and then decreases.

After corrosion, the surface of AM as-built samples has many pits in comparison with the conventional as-built samples because of non-equilibrium phase present in the AM as-built samples, which leads to the formation of a less protective passive layer. In the as-built samples, the stressed regions due to presence of non-equilibrium phase allow the

surface to dissolve easily. The observed results are consistent with XPS results shown in Figure 5.13 and Table 5.6. The available surface flaws are the main reason for corrosion pits in the as-built samples, which break the passive films.

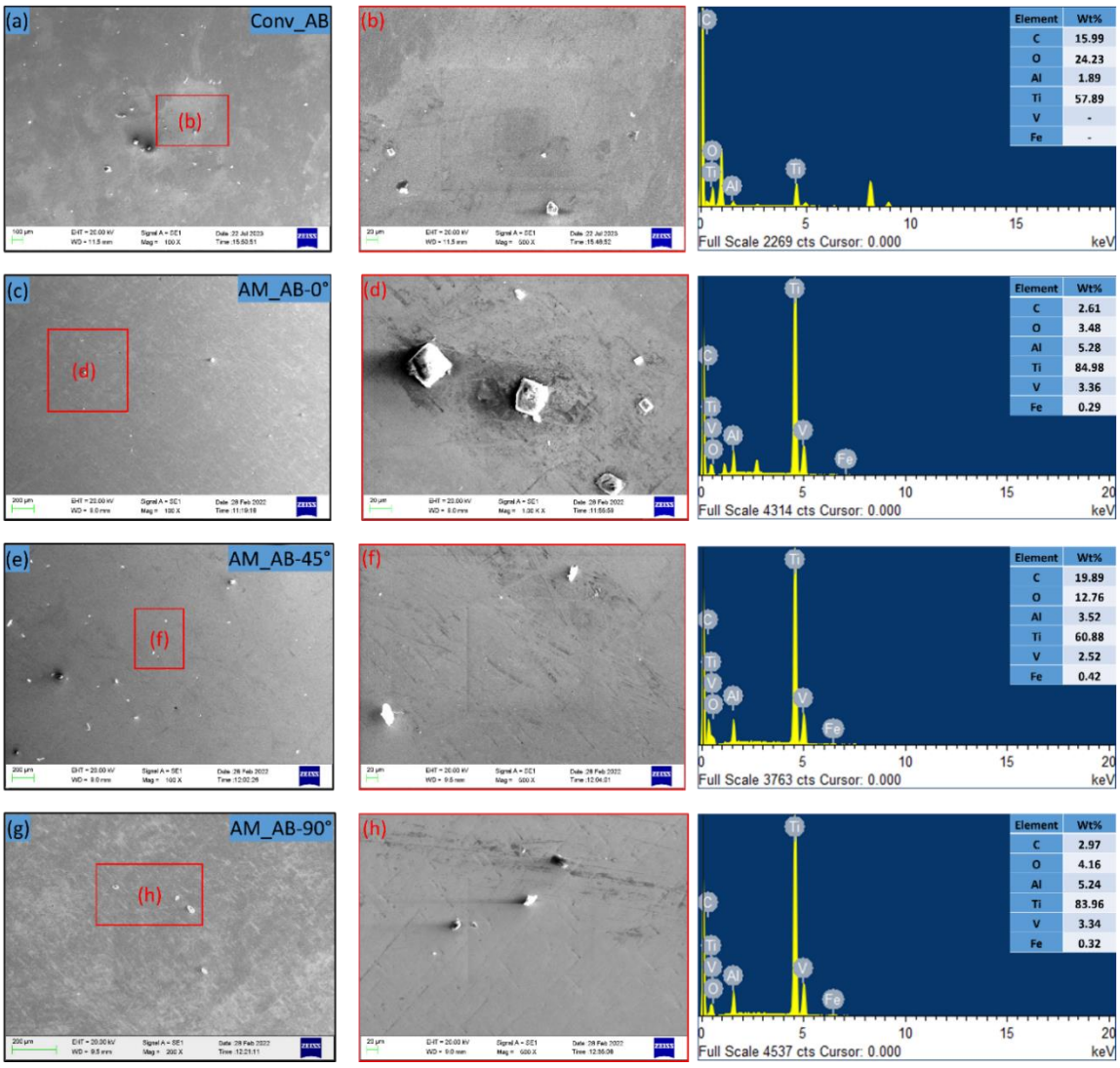

Figure 5.16 SEM with EDS of corroded regions of as-built conventional and AM samples: (a, b) conventional, (c, d) AM 0°, (e, f) AM 45°, and (g, h) AM 90°

However, after the heat treatment, the localised corrosion becomes less severe. Figure 5.17 presents surface morphology of the heat-treated conventional (Figure 5.17 (a) and (b)), AM 0° (Figure 5.17 (c) and (d)), AM 45° (Figure 5.17 (e) and (f)), and AM 90° (Figure 5.17 (g) and (h)) corroded samples. Figure 5.17 also presents the weight

percentage of different elements available on the corroded conventional and AM heat-treated samples. The surface behaviour of the HT samples is nearly similar to that of samples conventionally manufactured. The results obtained from Tafel plots (Table 5.4) validate this observation, which is also consistent with the previous studies [128, 208].

Figure 5.17 (a) presents corroded surface of the conventional heat-treated samples where non protective corrosion layer is formed on the whole surface. In the AM heat-treated samples, the formation of the β phase in place of the needle-type strained martensitic phase improved the corrosion performance and formed highly protective passive layer [13]. The oxide layers formed on the surface of the samples are not conductive, which improves the corrosion potential and decreases the corrosion rate. The observed results are consistent with the electrochemical properties obtained from Tafel plots shown in Table 5.4.

It is evident from the above discussion that Ti-6Al-4V with β phase sample has better corrosion resistance than Ti-6Al-4V with α phase because of stable oxide films formed on the surface of heat-treated samples [134]. As the build orientation increases from 0° to 90°, the weight percentage of oxygen initially increases and then decreases. According to Figure 5.17 (d), (f), and (h), flake type corrosion pits are observed in heat-treated samples. Other researchers have also observed that mechanical defects like inclusions, cracks, and pores are the main cuse of corrosion pits on the surface of metal alloys, as a result, corrosive solution may find it easier to penetrate the Ti-6Al-4V alloy [128, 132].

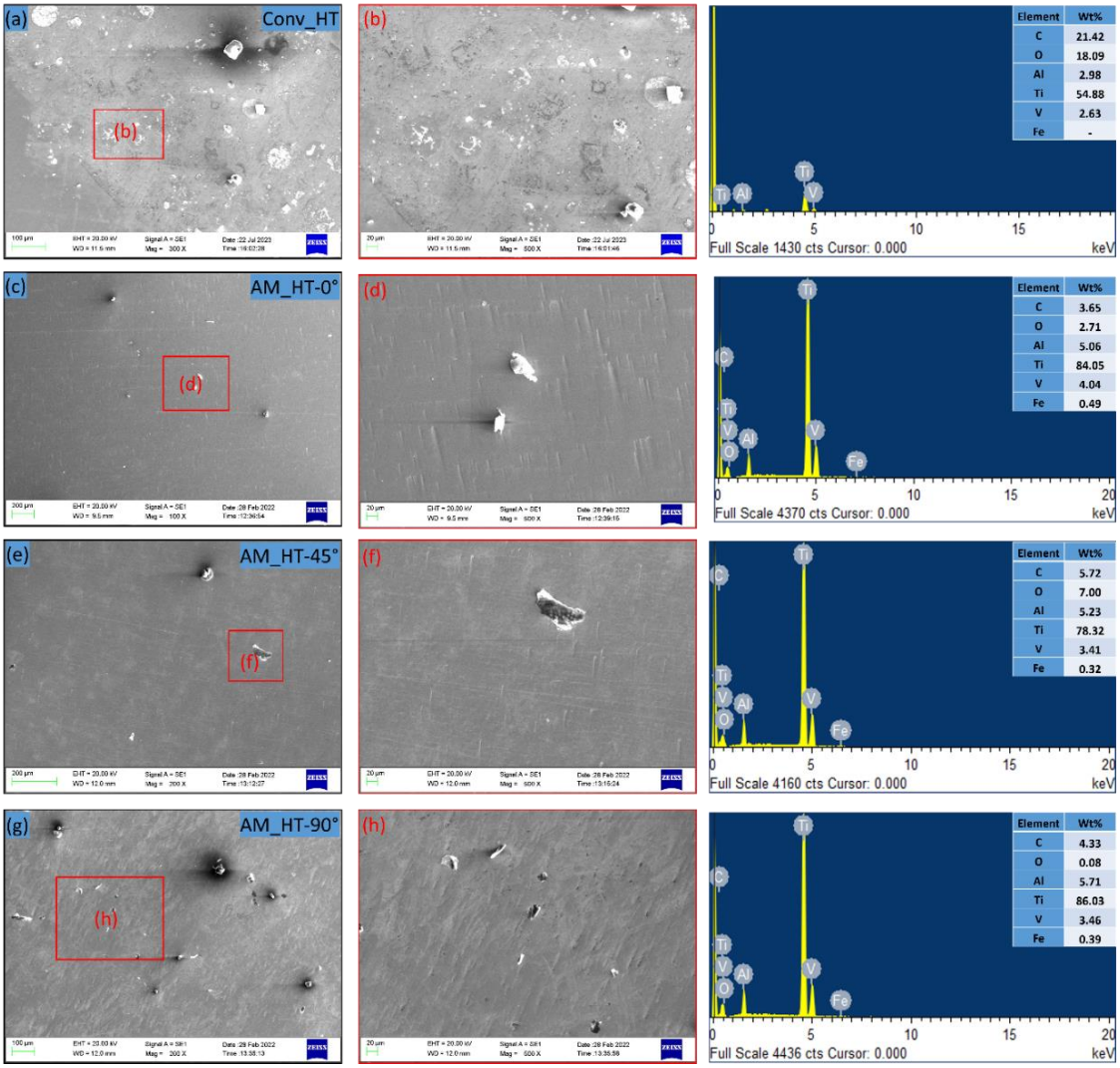

Figure 5.17 SEM with EDS of corroded regions of heat-treated conventional and AM samples: (a, b) conventional, (c, d) AM 0°, (e, f) AM 45°, and (g, h) AM 90°

With the above results and discussion of corrosion behaviour of AM fabricated Ti-6Al-4V alloy, results and discussion of wear and biological behaviour of AM fabricated Ti-6Al-4V alloy has been discussed in chapter 6.